Developmental Biology 382 (2013) 293–301

Contents lists available at ScienceDirect

Developmental Biology

journal homepage: www.elsevier.com/locate/developmentalbiology

Genomes and Developmental Control

Combined function of *HoxA* and *HoxB* clusters in neural crest cells

Maxence Vieux-Rochas [a], Bénédicte Mascrez [b], Robb Krumlauf [c,d], Denis Duboule [a,b,*]

[a] School of Life Sciences, Federal Institute of Technology (EPFL) Lausanne, Switzerland
[b] Department of Genetics and Evolution, University of Geneva, Sciences III, Switzerland
[c] Stowers Institute for Medical Research, Kansas City, MO 64110, USA
[d] Department of Anatomy and Cell Biology, University of Kansas Medical Center, Kansas City, KS 66160, USA

ARTICLE INFO

Article history:
Received 26 June 2013
Accepted 27 June 2013
Available online 11 July 2013

Keywords:
Hox genes
Craniofacial
Thymus
Dentary bone
Neural crest cells.

ABSTRACT

The evolution of chordates was accompanied by critical anatomical innovations in craniofacial development, along with the emergence of neural crest cells. The potential of these cells to implement a craniofacial program in part depends upon the (non-)expression of *Hox* genes. For instance, the development of jaws requires the inhibition of *Hox* genes function in the first pharyngeal arch. In contrast, *Hox* gene products induce craniofacial structures in more caudal territories. To further investigate which *Hox* gene clusters are involved in this latter role, we generated *HoxA*;*HoxB* cluster double mutant animals in cranial neural crest cells. We observed the appearance of a supernumerary dentary-like bone with an endochondral ossification around a neo-Meckel's cartilage matrix and an attachment of neo-muscle demonstrating that *HoxB* genes enhance the phenotype induced by the deletion of the *HoxA* cluster alone. In addition, a cervical and hypertrophic thymus was associated with the supernumerary dentary-like bone, which may reflect its ancestral position near the filtrating system. Altogether these results show that the *HoxA* and *HoxB* clusters cooperated during evolution to lead to present craniofacial diversity.

Introduction

In the course of evolution, the emergence of a new head allowed for an important transition in the feeding behavior, from a filtrating to a masticating strategy. Subsequently, the acquisition of jaws played a role in developing predation behaviors in vertebrates. While paleontological studies have led to serial reconstructions of the progressive modifications in bone shapes, which could account for such a huge morphological re-organization, the molecular and cellular regulatory mechanisms underlying these processes remain unclear. It is however believed that the acquisition of the head was made possible by the appearance of cranial neural crest cells (CNCCs), a novel cell type with extensive potential for migration, proliferation and differentiation into a wide variety of cell types (Creuzet et al., 2005; Kontges and Lumsden, 1996; Kuratani, 2012; Kuratani et al., 2013).

Detailed cell-lineage analyses in chicken and mouse have provided a comprehensive description and understanding of both the fates of these cells and the diverse processes and pathways governing their migration (Couly et al., 1993; Santagati and Rijli, 2003; Theveneau and Mayor, 2012). Furthermore, studies in a number of vertebrate model systems have begun to elucidate the cellular and molecular mechanisms underlying the formation of CNCC and onset of craniofacial morphogenesis (Gammill and Bronner-Fraser, 2002; Meulemans and Bronner-Fraser, 2004; Milet and Monsoro-Burq, 2012; Prasad et al., 2012). CNCCs have a specific gene regulatory network, which is conserved between species but different from other NCCS (Sauka-Spengler and Bronner-Fraser, 2008) and many types of tissue derivatives of CNCCs are restricted to craniofacial territories, such as their capacity to form bones and connective tissues. However, trunk NCCs have the potential to form some cell types characteristic of CNCCs after long-term in vitro culture in association with the loss of *Hox* genes function (Santagati and Rijli, 2003). Therefore, both an intrinsic genetic program and extrinsic environmental signals co-evolved to specify a subset of the NCCs and prevent them from altering the development of more rostral parts of the body.

Hox genes were proposed to encode the major inhibitors of the craniofacial program carried by CNCC (Couly et al., 1998). As a consequence, their functional inhibition in pharyngeal arches (PAs) is an essential condition for proper jaw formation(Couly et al., 2002). In particular, *HoxA* cluster genes are considered as the principal functional antagonist against craniofacial programs. A prevalent role is played by *Hoxa2* as its inactivation in mouse induced a mirror-image duplication of the lower jaw with two Meckel's cartilage (Gendron-Maguire et al., 1993; Rijli et al., 1993) and that other *Hox2* paralogs, such as *Hoxb2*, in zebrafish may cooperate

* Corresponding author at: School of Life Sciences, Federal Institute of Technology (EPFL) Lausanne, Switzerland. Fax: +41 22 379 6795.
E-mail addresses:
Denis.Duboule@unige.ch, Denis.Duboule@epfl.ch (D. Duboule).

0012-1606
http://dx.doi.org/10.1016/j.ydbio.2013.06.027

with *Hoxa2* in the second pharyngeal arch (Hunter and Prince, 2002). In addition, mice carrying mutations for both *Hoxa1* and *Hoxb1* indicate synergy between these genes in branchial arch patterning and the generation of cranial neural crest(Gavalas et al., 2001; Minoux et al., 2009). The functional redundancy between *Hox* clusters could thus mask some of the properties of each cluster.

Interestingly, the evolution of craniofacial morphologies occurred along with the two rounds of genome duplication (2R), at the root of modern vertebrates (Kuraku et al., 2009; Oisi et al., 2013; Shimeld and Donoghue, 2012; Smith et al., 2013). It is thus believed that CNCCs and their many functional features have appeared due to neo-functionalization events (Sauka-Spengler et al., 2007; Yu et al., 2008), which potentially followed the successive genomic duplications in parallel with the progressive modification of the rostral parts of the embryos, such as the acquisition of a new motile neck and the modern jaws. The resulting functional overlaps between gene clusters may also help to explain why mutant animals carrying a deletion for a single *Hox* gene cluster exhibit rather mild phenotypes. However, while the complete deletion of the *HoxA* gene cluster in crest cells gave a phenotype stronger than the deletion of *Hoxa2* alone (Minoux et al., 2009), its combination with the removal of the entire *HoxD* cluster did not strongly increase the severity of defects in craniofacial development (Minoux et al., 2009). This suggests that different *Hox* gene clusters may participate in the development of distinct tissues or structures and that *Hoxd* genes have little functional impact upon CNCCs.

The time sequence in *Hox* gene cluster duplication has been a matter of conflicting interpretations. Because the ((A,B):(C,D)) model was nevertheless proposed as the most parcimonious (Ravi et al., 2009), the *HoxA* and *HoxB* clusters may have a closer phylogenetic relationship and hence share more functionalities than with either of the other two clusters (*HoxC* and *HoxD*) (Ravi et al., 2009). In this model, it would be reasonable to expect that some regulatory or functional traits, which evolved after the first whole genome duplication, might be conserved in both twin-loci, after the second round of genome duplication. We investigated this hypothesis with respect to head formation by generating double *HoxA*;*HoxB* mutant mice. Because the deletion of the *HoxA* cluster is embryonic lethal, we used a conditional allele together with a *Wnt1*:CRE deleter strain. The *Wnt1* promoter was shown to be active mostly in the early cranial neural crest cells, thus leading to the specific deletion of all *Hoxa* genes in this cellular pool ($HoxA^{c/c}$;*wnt-cre*)(Minoux et al., 2009). We focused our analyses on the function of both the *HoxA* and *HoxB* clusters during craniofacial morphogenesis and compared the full *HoxA* mutant phenotype in CNCCs with the phenotype of double $HoxA^{c/c}$;$HoxB^{del/del}$;*wnt-cre* mutant mice. We found a strong re-enforcement in the double mutant, with the appearance of a second dentary bone-like structure with an endochondral ossification around a cartilaginous matrix, the classical hallmarks of a Meckel's cartilage. We also observed an abnormal migration (or lack thereof) of a part of a hypertrophic thymus in double mutant mice, resembling a primitive form of the cervical thymus. $HoxA^{c/+}$;$HoxB^{del/del}$;*wnt-cre* embryos also displayed a triplication of the stapes, in the middle ear. These findings provide insight into functional relationships between duplicated *Hox* clusters and uncover some of the shared functional roles for the *HoxA* and *HoxB* clusters in patterning CNCC derivatives.

Material and methods

Mice and mating

The floxed *HoxA, Wnt1::Cre* and *HoxB* mice were described previously (Danielian et al., 1998; Kmita et al., 2005; Medina-Martinez et al., 2000). Mutant fetuses were produced by crossing $HoxA^{flox/+}$;$HoxB^{del/+}$ or $HoxA^{flox/flox}$;$HoxB^{del/+}$ females with $HoxA^{flox/+}$;$HoxB^{del/+}$;*wnt-cre* or $HoxA^{del/+}$;$HoxB^{del/+}$;*wnt-cre* males.

Skeletal preparations and histological sections

Cartilage staining of E14.5 embryos as well as bone and cartilage staining of E18.5 embryos were carried out as previously described (Vieux-Rochas et al., 2007). Serial histological sections of E18.5 fetuses were treated with Vieux-Rochas quadrichromic staining. Slides were put in Celestine blue solution during 5 min and washed twice in dH_2O. Slides were then put in tartrazine solution of 0.25% for 5 min and washed twice in dH_2O followed by 2 min in lithium carbonate solution 0.03% and 1 min in methyl blue/Fuchsine acid solution. Slides were treated 2 min in 1% acetic acid solution and dehydrated in alcohol bath. Apoptosis was analyzed on histological sections of E15,5 embryos using the in situ cell death detection kit of Roche with the TUNEL technology.

3D reconstruction and OPT

A Leica DM5500 microscope was used for its multishot function of serial slides. Movies reconstruction was processed with Fiji plug in of ImageJ. Optical Projection Tomography (OPT) (http://www.bioptonics.com/) was used to generate 3D reconstruction of skeletal preparation.

Results and discussion

Function of the HoxA cluster in craniofacial morphogenesis

The constitutive inactivation of the entire *HoxA* cluster is early lethal and hence we used a conditional allele ($HoxA^{c}$) to generate mice either lacking *HoxA* function alone, or mutant for both *HoxA* and *HoxB* clusters. The use of either the two *HoxA* conditional alleles ($HoxA^{c/c}$), or of one full deleted and one conditional allele ($HoxA^{Del/c}$) gave the same phenotypes when combined with the *wnt-cre* transgene. This indicates that the cre deleter transgene was equally efficient with either one or two floxed *HoxA* alleles and that major *HoxA* functions are restricted to CNCCs. In a previous series of analyses describing the craniofacial phenotype of mutant mice lacking all *HoxA* function in crest cells, either with or without the presence of the *Hox*D cluster (Minoux et al., 2009; Minoux and Rijli, 2010), a strong phenotype was associated with the deletion of *HoxA* in NCCs, more severe than those observed in either one of the *Hoxa1* (Carpenter et al., 1993; Mark et al., 1993), *Hoxa2* (Gendron-Maguire et al., 1993; Rijli et al., 1993) or *Hoxa3* (Chisaka and Capecchi, 1991) single mutant mice. These latter mice displayed craniofacial deformations in hindbrain derivatives, in the middle ear and in PA2-derivatives, respectively, indicating that multiple *Hoxa* genes participate in craniofacial patterning.

In addition to the duplication of Meckel's cartilage also described in *Hoxa2* mutant mice (Gendron-Maguire et al., 1993; Rijli et al., 1993), $HoxA^{c/c}$;*wnt*-cre specimen displayed a severe defect illustrated by an ectopic cartilage starting near the *pars canalicularis* and extending up to the hyoid cartilage in a rostro-caudal direction. Likewise, an ectopic junction between the hyoid cartilage and the thyroid cartilage is present in the $HoxA^{c/c}$;*wnt*-cre mice. These ectopic cartilages were previously interpreted as supernumerary Meckel's cartilages (Minoux et al., 2009). While this is indeed a genuine possibility, we re-visited some aspects of this phenotype. Indeed a similar junction between the great horn of the hyoid (*ghh*) and the thyroid (*th*), which was initially not described in *Hoxa3* mutant mice (Chisaka and Capecchi, 1991), was noted in other studies (Chen et al., 2010; Condie and Capecchi,

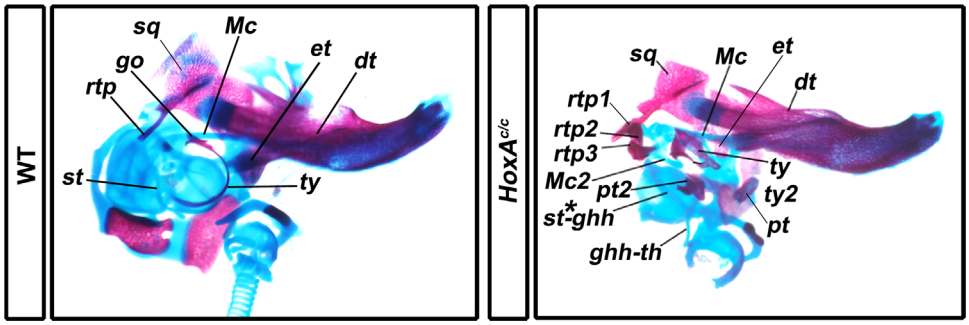

Fig. 1. Phenotype of *HoxA*$^{c/c}$;*wnt-cre* mutant mice. Dissection of a E18,5 wild-type dermatoskeleton (left) compared to a E18,5 old *HoxA*$^{c/c}$;*wnt-cre* mutant embryo (right). Only those structures derived from the lower jaw and the neck are shown and tentatively identified. Left. *dt*, dentary; *et*: ethmoide; *go*: gonial bone; *Mc*, Meckel's cartilage; *rtp*: retrotympanic process; *st*, styloid; *sq*, squamosal bone; *ty*: tympanic bone. Right. *rtp2* and *rtp3*; duplication and triplication of the retrotympanic process. *Mc2*, duplication of Meckel's cartilage; *st***-ghh*: stylo-like-great horn hyoid junction; *ghh-th*: great horn hyoid-thyroid junction; *ty*: tympanic bone; *ty2*: duplicated tympanic bone; *pt*: pterygoid bone; and *pt2*: duplicated pterygoid bone.

1994; Manley and Capecchi, 1997), suggesting that this ectopic cartilage structure may derive from the hyoido-thyroid junction, which is specific to *Hoxa3* mutant mice (Fig. 1; the *ghh-th* junction).

Likewise, in some instances, the ectopic cartilage starting near the *pars canalicularis* showed an attachment to this latter structure, at a position where the styloid is normally attached. Because this cartilage does not appear to be formed proximally by an ectopic malleus, the possibility exists that this resulting bipartite cartilage may be partly made of a genuine styloid (*st*) cartilage. Consequently, and in the absence of a definitive identification, we refer to this cartilage as a junction between a 'styloid-like' and the great horn of the hyoid cartilage (Fig. 1, the *st***-ghh* junction). Also in our *HoxA*$^{c/c}$;*wnt*-cre mutant mice, an endochondral ossification of this cartilage was not observed, unlike in a genuine Meckel's cartilage, which has a dorso-ventral orientation, rather than the scored rostral to caudal orientation. This connection is present in many vertebrates and reported as stylohyal (Owen, 1866). It is also observed in human affected by the Eagle syndrome (Eagle, 1949) or in retinoic acid-treated mice (Vieux-Rochas et al., 2007). The observation that in the *HoxA*$^{c/c}$;*wnt*-cre mutant the NCCs derivatives of PA2 to PA4 are somewhat distinct from those in PA1 implies that *Hoxa* genes alone are not sufficient to impose a full transformation of the PA2 to PA4 into a PA1 *Hox*-free genetic ground-state and suggests that other *Hox* clusters may participate to this functional task.

Phenotypic analyses of NCC conditional HoxA;HoxB mutant mice

We compared the *HoxA* phenotype with skeletal analyses of the *HoxA*$^{c/c}$;*HoxB*$^{del/del}$;*wnt*-cre double mutant mice. A supernumerary bone was found in the neck region of the latter (Fig. 2A bottom; *dt**, Suppl. movies 1, 2). This novel structure of cylindrical shape was positioned laterally when compared to the hyoid bone (Fig. 2A, bottom). It was attached to an additional piece of cartilage, which originated from the styloid-like-hyoid junction (Fig. 2B). This bone presented two cartilaginous structures on its most dorsal part, referred to as a putative duplicated angular and condylar processes (Fig. 2A bottom; black and red arrowhead). Histological analyses revealed the presence of cartilage within the bone itself, suggesting that it originated via endochondral ossification (Fig. 2C bottom). Finally, we observed the attachment of a muscle directly to this supernumerary bone (Fig. 2C bottom; green arrow), much like the muscle attachment to the endogenous dentary bone. Consequently, we propose to refer to this bone as a supernumerary dentary-like bone (Fig. 2A; asterisk and Fig. 2B,C; *dt**). Accordingly, the small piece of cartilage is considered as a quadruplicated Meckel's cartilage (Fig. 2B bottom; see the *Mc4**). Another piece of cartilage was found in close contact with the existing modified middle ear, similar to the situation in the *Hoxa2* mutant mice (Gendron-Maguire et al., 1993; Rijli et al., 1993), with a cartilage rod carrying a protuberance, proximally (Fig. 2B bottom). The proximal protuberance of this cartilage could be interpreted as a triplicated malleus, which is a subdivision of the Meckel's cartilage. Thus, we propose to refer to this cartilage as a triplicated Meckel's cartilage-like and a triplicated malleus (Fig. 2B; *Mc3** and *ma3**).

Supplementary material related to this article can be found online at http://dx.doi.org/10.1016/j.ydbio.2013.06.027.

The analyses of intermediate allelic combinations systematically revealed a transient transformation of PA2 into a pseudo-PA1. For example, *HoxA*$^{c/+}$;*HoxB*$^{del/del}$;*wnt*:cre exhibited more severe defects in bone formation as compared to *HoxA* homozygous mutant mice. However, this particular mutant did not develop any real bone in close contact with the supernumerary cartilage (Fig. S1).

Functional overlaps between HoxA and HoxB clusters

Targeted mutations of *Hoxa* and *Hoxb* genes have rarely elicited comparable phenotypes and hence these two gene clusters may display a reduced functional equivalence, at least when early developmental stages are considered (Soshnikova et al., 2013). The supernumerary bone found in *HoxA*$^{c/c}$;*HoxB*$^{del/del}$;*wnt-cre* animals, absent from our *HoxA*$^{c/c}$ mutant mice, indicate that some functional redundancy exists between these two clusters in the context of the PA2 derivatives of NCCs. This is in agreement with recent studies of the *elephant shark Hox* clusters, that suggest a (AB:CD) sequence in the temporal order of *Hox* cluster duplication (Ravi et al., 2009), along with the two rounds of whole-genome duplication (2R).

We further addressed this issue by generating *HoxB*$^{del/del}$ or *HoxB*$^{del/+}$ mutant mice carrying either a full (non-conditional) deletion allele of the *HoxA* cluster with or without the *HoxA* conditional allele and its *wnt-cre* deleter transgene. *HoxA*$^{del/c}$;*HoxB*$^{del/del}$;*wnt-cre* embryos were however not observed amongst 18.5 days old fetuses, likely due to premature lethality (Soshnikova et al., 2013). We thus generated *HoxA*$^{del/c}$;*HoxB*$^{del/+}$;*wnt-cre* mutant embryos. These specimens showed a bone at E18.5, which resembled the supernumerary duplicated-dentary bone scored in mice double homozygous for the deletion of *HoxA* and *HoxB* in NCCs (Fig. S2; asterisk). No cartilage was found in close contact with this novel bone and histological analyses did not reveal a cartilagenous structure inside. Consequently, we did not consider this bone as a genuine, second dentary bone-like structure. Because the ectopic nodules of ossification characterized in the *HoxA*$^{c/c}$;*wnt-cre* mutant embryo were not re-enforced when removing one copy of *HoxB* (in *HoxA*$^{c/c}$;*HoxB*$^{del/+}$;

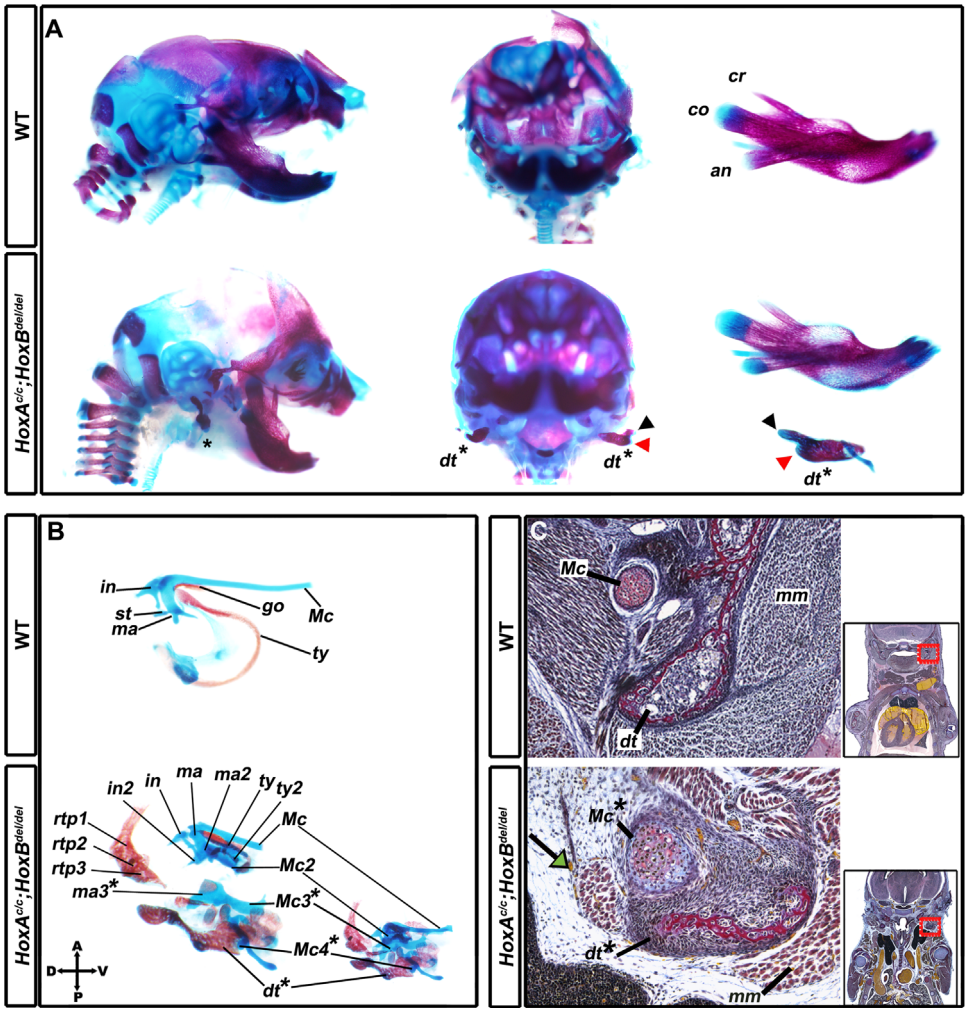

Fig. 2. A duplicated dentary-like bone in *HoxA*$^{c/c}$;*HoxB*$^{del/del}$;*wnt-cre* mutant mice. (A) Lateral (left) and frontal (right) views of wild-type (top) and double *HoxA*$^{c/c}$;*HoxB*$^{del/del}$;*wnt-cre* (bottom) E18,5 mutant head skeletons. The supernumerary bone formed in the *HoxA*$^{c/c}$;*HoxB*$^{del/del}$;*wnt-cre* mutant embryo near the hyoid bone is interpreted as a duplicated dentary bone (bottom, *dt**). Two protuberances are present on the extremity of this duplicated dentary bone, interpreted as the condylar (black arrowhead) and the angular (red arrowhead) processes. an, angular process; co, condylar process; cr,coronoid process; *dt**, duplicated dentary bone (B) Dissected middle ears from a wild-type (top) and a double *HoxA*$^{c/c}$;*HoxB*$^{del/del}$;*wnt-cre* mutant (bottom) embryos. On the bottom right, the sample is shown before dissection. Top, *in*, incus; *st*, styloid; *ma*, malleus; *go*, gonial bone; *ty*, tympanic bone. Bottom. *dt**, duplicated dentary bone; *ma2*, *ma3**, duplicated and triplicated malleus; *Mc2*, *Mc3**, *Mc4**, duplicated, triplicated and quadruplicated Meckel's cartilages. The triplicated malleus (*ma3**) remains as a cartilage, whereas the quadruplicated Meckel's cartilage (*Mc4**) is comprised within a bone matrix corresponding to the dentary bone (*dt*); *ghh-th*: great horn hyoid-thyroid junction; *rtp1*, retrotympanic process; *rtp2*, *rtp3*, duplicated and triplicated retrotympanic process; *sq*, squamosal bone; *sq2*, *sq3*, duplicated and triplicated squamosal bone; *st*, styloid; *st***-ghh*: stylo-like-great horn hyoid junction; *ty*, tympanic bone; *ty2*, duplicated tympanic bone. (C) Dissection of the duplicated dentary-like bone present in *HoxA*$^{c/c}$;*HoxB*$^{del/del}$;*wnt-cre* mutant mice (bottom) compared to the wild-type dentary bone (top).

wnt-cre mutant embryos), the supernumerary bone observed in *HoxA*$^{del/c}$;*HoxB*$^{del/+}$;*wnt-cre* embryo likely illustrates a function of the *HoxA* cluster in epithelia, i.e. outside the NCCs contingent. It also underscored the prevalent role of *Hoxa* genes in PAs differentiation (Minoux et al., 2009).

Interestingly in the *HoxA*$^{c/+}$;*HoxB*$^{del/del}$;*wnt-cre* mice, we observed a modification of the proximal part of the styloid (Fig. 3; *sp2, sp3*). In these mutant mice, the styloid is also detached from the *pars canalicularis* with a proximal modification of its shape. However, in some embryos, neo cartilages are formed and are detached from the styloid cartilage, yet they remain in close contact. We thus identified these anatomical pieces as putative triplication of the stapes (Fig. 3; *sp2, sp3*). This phenotype was not scored neither in the middle ears of *HoxA*$^{c/+}$ animals, nor in *HoxB*$^{del/del}$ mutant embryos. In contrast, the absence of stapes was reported both in *Hoxa2* (Gendron-Maguire et al., 1993; Rijli et al., 1993) and in double *Hoxa1*;*Hoxb1* (Rossel and Capecchi, 1999) mutant mice. Because the stapes derive from PA2, whereas the incus is derived from PA1 (O'Gorman, 2005), the absence of stape in the *Hoxa2* (Gendron-Maguire et al., 1993; Rijli et al., 1993) and in double *Hoxa1*;*Hoxb1*(Rossel and Capecchi, 1999) mutant mice was associated with a problem of PA2 formation. The potential triplication of the stapes in the *HoxA*$^{c/+}$;*HoxB*$^{del/del}$;*wnt-cre* mutant embryos suggests that some *Hoxb* genes may exert specific functions during the formation of the middle ear within PA2.

The triplication of stapes suggests a gain rather than a loss of function for the *Hoxa2* gene product and hence multiple stapes-like structures in *HoxA*$^{c/+}$;*HoxB*$^{del/del}$;*wnt-cre* mutant embryo may reflect a specific functional antagonism between *Hoxb* genes and *Hoxa2*, whereby the potential of *Hoxa2* to multiply the number of stapes would be restricted by *Hoxb* gene function. This is supported by the absence of supernumerary stapes either in the *HoxA*$^{c/c}$;*HoxB*$^{del/del}$;*wnt-cre* and in *HoxA*$^{c/c}$;*wnt-cre* or in *HoxA*$^{c/+}$;*wnt-cre* mutant embryos. In this view, however, one may have expected additional stapes to occur in full *HoxB* mutant mice, which was not the case. Such opposite functions between the *HoxA* and the *HoxB* clusters have already been reported to occur

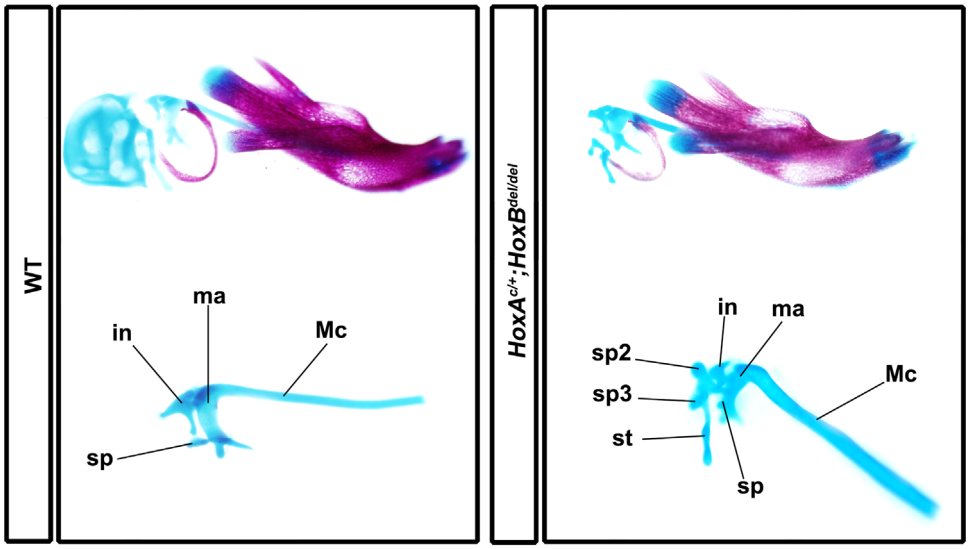

Fig. 3. Functional redundancy between *HoxA* and *HoxB* clusters. Dissection of the dentary bone and middle ear of a wild-type (left) and $HoxA^{c/c}$;$HoxB^{del/del}$;*wnt-cre* mutant (right) embryos at E18,5. In the $HoxA^{c/c}$;$HoxB^{del/del}$;*wnt-cre* mutant embryo, the middle ear is severely modified with two protuberances around the stape (*sp2*, *sp3*). Due to their shapes and positions, they are tentatively identified as duplicated and triplicated stapes.

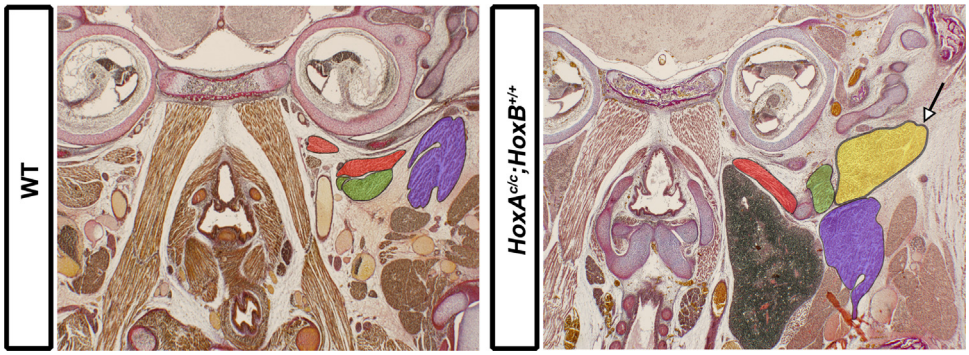

Fig. 4. Reorganization of muscles in the $HoxA^{c/c}$, $HoxB^{del/del}$;*wnt-cre* mutant embryo. (A, B) In $HoxA^{c/c}$;$HoxB^{del/del}$;*wnt-cre* mutant embryos, a duplication of the sternocleidomastoid muscle is observed (yellow and white arrows). The orientations of both the stylohyoidus and digastric muscles are also modified in the mutant embryo when compared to wild-type (in red and green, respectively), whereas the duplicated stream of the sternocleidomastoid muscle has a normal orientation (in purple). (C, D) Neo-formation of a muscle attached to the duplicated dentary bone. Wild-type (C) and mutant (D) views. The novel Meckel's cartilage (*Mc**) is embedded within the duplicated dentary bone (*dt**), which displays an endochondral ossification. At the distal extremity of the duplicated dentary bone, a muscle is formed *de novo* (white arrow). *dt*: dentary; *dt**: duplicated dentary bone; *hy*: hyoid bone; *in*: incus; *ma*: malleus; *Mc*: Meckel's cartilage; *Mc**: duplicated Meckel's cartilage; *mm*: masseter muscle; *sp*: stapes; *sp2*: duplicated stapes; *sp3*: triplicated stapes; *st*: Styloid; purple, sternocleidomastoid muscle; red, stylohyoidus muscle; green, digastric muscle; yellow, duplicated sternocleidomastoid muscle.

between *Hoxa2* and *Hoxb2* during hindbrain oligodendrocyte patterning (Miguez et al., 2012) and may suggest that the *HoxA* cluster has a primary role during middle ear formation, whereas *Hoxb* genes serve to fine-tune some of the morphological readouts controlled by *HoxA*.

Changes in muscle organization

To complement and strengthen the analysis of $HoxA^{c/c}$;$HoxB^{del/del}$;*wnt-cre* mutant cartilages and bones, we determined the pattern of muscles attached to the observed supernumerary bone. While no muscular abnormality was observed in *HoxB* mutant animals, $HoxA^{c/c}$;*wnt-cre* specimen clearly exhibited an abnormal muscle organization. $HoxA^{c/c}$;*wnt-cre* mutant embryos indeed presented a duplication of the sternocleidomastoid muscle (Fig. 4; arrow) such that two streams of muscle fibers were apparent, the expected wild type muscle (Fig. 4 right; purple) and an other muscle (Fig. 4 right; yellow) sharing with the normal stream a unique rostral attachment (Suppl. movies 3–5). The caudal attachment, however, was different from the additional stream, ending near the tentatively identified stylo-hyoid connection (Suppl. movies 3–5). Together, these data tentatively identify this muscle as a duplicated sternocleidomastoid (Fig. 4 right; arrow).

Supplementary material related to this article can be found online at http://dx.doi.org/10.1016/j.ydbio.2013.06.027.

In $HoxA^{c/c}$,$HoxB^{del/del}$;*wnt-cre* mutant specimen, while the sternocleidomastoid muscle was similarly duplicated, a supernumerary muscle was formed *de novo*, attached to the distal part of the neo-dentary-like bone (Fig. 2C; arrow). This supernumerary muscle displayed a rostro-caudal growth and was the only duplicated muscle observed in such mutant embryos. Since most cranial muscles derive from splanchnic or paraxial mesoderm, we infer that the depletion of *Hoxa* genes from NCCs along with the deletion of *HoxB* led to modifications in mesoderm patterning, inducing *de novo* muscle formation and hence this suggests that a cross-talk exists between cranial neural crest cells and the mesoderm (Rinon et al., 2007). As $HoxB^{del/del}$ mutant embryos did not present any duplicated muscle, we conclude that the inactivation of *Hox*a and *Hoxb* genes in neural crest cells caused these profound modifications in muscle patterning, likely triggered by supernumerary bones and cartilages.

Table 1
Summary of malformations obtained in the different genotypes. Unilateral ectopic and hypertrophic thymuses were found only in the *HoxA$^{c/c}$;wnt-cre* mutant embryos, whereas bilateral ectopic and hypertrophic thymuses were identified in both *HoxA$^{c/c}$;HoxB$^{del/del}$;wnt-cre* and *HoxA$^{c/c}$;HoxB$^{del/+}$;wnt-cre* mutant embryos. Triplicated stapes were observed in the *HoxA$^{c/+}$;HoxB$^{del/del}$;wnt-cre* mutant embryos. The neo-duplicated dentary bone was scored in the *HoxA$^{c/c}$;HoxB$^{del/del}$;wnt-cre* mutant embryos, whereas pseudo-dentary bone without cartilage connection were present in the *HoxA$^{c/c}$;HoxB$^{del/+}$;wnt-cre* mutant embryos. Finally muscle duplications were identified in *HoxA* cluster mutants, with or without deletion of the *HoxB* cluster.

	HoxA$^{c/c}$	*HoxA$^{c/c}$;HoxB$^{del/del}$*	*HoxA$^{c/c}$;HoxB$^{del/+}$*	*HoxA$^{c/+}$;HoxB$^{del/del}$*
Unilateral ectopic and hypertrophic thymus	2/2	0	0	0
Bilateral ectopic and hypertrophic thymus	0	4/4	5/5	0
Triplicated stapes	0	0	0	6/7
Neo-duplicated-dentary bone	0	3/3	0	0
Neo-bone without cartilage connection	0	0	3/3	0
Muscle duplication and modification	2/2	3/3	3/3	0

Ectopic and hypertrophic thymus

Ectopic cervical position of thymic tissue occurs in BALB/c and C57BL/6 mice (50% and 33%, respectively) (Dooley et al., 2006). However, it was never observed in the B6CBAF1 genetic background, which is used to backcross all of our mutant stocks for generations. Surprisingly, we observed a unilateral hypertrophic thymus in *HoxA$^{c/c}$;wnt-cre* mutant mice (Fig. 4 right; see also Table 1). This phenotype was enhanced in both *HoxA$^{c/c}$;HoxB$^{del/+}$;wnt-cre* and *HoxA$^{c/c}$;HoxB$^{del/del}$;wnt-cre* animals, where hypertrophic thymuses were observed bilaterally (Fig. 5A–C). These thymuses started rostrally near the top of the pharynx and extended caudally down to their expected position in the anterior mediasta, above the heart (see scheme in Fig. 6C and movies 3–5). Therefore, a part of the thymus appeared to have migrated normally, whereas another region was retained at a cervical position. However, no gross anatomical malformation of the thymus itself was observed and all animals analyzed displayed wild type medulla and cortex, as well as Hassal's corpuscule.

This apparent extension of the thymus may derive from a defect in the mechanism that separates the thymic primordium from the pharynx. In birds and some fishes indeed, the thymus does not migrate and stays attached to the pharynx (Grevellec and Tucker, 2010; Lam et al., 2002; Le Douarin et al., 1984). However, neither *HoxA$^{c/c}$;HoxB$^{del/+}$;wnt-cre*, nor *HoxA$^{c/c}$;HoxB$^{del/del}$;wnt-cre* embryos at E18.5 present an attachment of the thymus to the pharynx in the cervical region (Fig. 5D, E). In this view, thymic cells would correctly migrate to their caudal position. One of the actors important for the migration of the thymus are neural crest cells (Foster et al., 2010). Moreover, a thymus defects were observed in early neural crest migration in *Hoxa1* mutants, though these appeared to be compensated for in later stages (Gavalas et al., 2001). As previously shown, neural crest cell migration was not grossly affected in *HoxA$^{c/c}$wnt-cre* mutant mice (Minoux et al., 2009), as at least part of the thymus was in the normal position. In addition, the thyroid gland, which is a PA2 derivative, was also found at the expected position (Fig. 5F, G; red arrow). The persistence of part of the thymus at a cervical level may result from a delay in the detachment of the thymus from the parathyroid gland and/or a decreased apoptotic activity between the thymic primordium and the pharynx. In one embryo only, the thymus was still attached to the pharynx at E18.5, on one side (Fig. S3), whereas in all other cases the cervical parts of the thymus had detached from both the pharynx and the parathyroid gland (Fig. 5D–G; green arrowhead). At E15.5, however, the thymus was still attached to the pharynx (Fig. 5H,I), a delay likely explained by a decrease or/and a delay in apoptosis normally occurring at E13.5, between the primordium and the pharynx This was supported by the few apoptotic cells in the pharynx endoderm, which were still observed at E15.5 leading to a full but delayed detachment between the pharynx and the thymus (Fig. S4; arrowhead).

We thus propose that the deletion of *HoxA* cluster genes may affect (directly or indirectly) the apoptotic process necessary to separate the thymus from the pharynx. Our results reveal that unlike the defects seen in CNCC migration of rhombomere 4 into PA2 in *Hoxa1/Hoxb1* double mutants (Gavalas et al., 2001), *HoxA/B* gene function is not required for the final migration of CNCCs in the thymus region. This is supported by the analyses of *HoxB$^{del/del}$* mice, which do not show any aberrant cervical thymus (Fig. S5 and (Medina-Martinez et al. (2000)). In this context, the defect observed in the migration of the thymus in either the *Hoxa3$^{del/+}$;Hoxb3$^{del/del}$;Hoxd3$^{del/+}$* or the *Hoxa3$^{del/+}$;Hoxb3$^{del/del}$;Hoxd3$^{del/del}$* compound mutant mice (Manley and Capecchi, 1998) may also be caused by the same delay in the separation of the thymic primordium from the pharynx, rather than by a perturbation in its migration.

Our data show that the selective depletion of both *HoxA* and *HoxB* gene function in cranial neural crest cells leads to profound anatomical modifications, affecting the proper patterning and/or positioning of cartilages, bones, muscles and thymus. While these results confirm that the abrogation of all *HoxA* function alone in NCCs tend to transform PA2, PA3 and PA4 towards the identity of PA1 (Minoux et al., 2009), the present analysis suggests that these transformations may not be fully complete and sufficient to generate the *Hox*-free environment necessary for the formation of the lower jaw (Minoux et al., 2009). In fact, while *HoxA$^{c/c}$;wnt*-cre mutant embryos indeed have a phenotype more severe than the defects associated with single *Hoxa2* mutant mice, the NCCs derivatives of PA2 to PA4 are still distinct from those in PA1, implying that *Hoxa* genes alone are not sufficient to impose a morphological ground-state to the former NCCs population. In a previous series of phenotypic analyses, the defects of *HoxA$^{c/c}$;wnt*-cre mice were not seriously aggravated when the *HoxD* cluster was also removed (Minoux et al., 2009). On the other hand, the *HoxC* cluster lacks most of the anterior *Hox* gene paralogs, which are instrumental in NCC specifications at the levels of PA2 to PA4. In contrast, our data indicates that *HoxB* cluster genes share some functional capacities with *HoxA* genes and thus help organizing structures in more rostral part of the branchial apparatus. The unability of PA2 to PA4 to form a full duplicated dentary bone could be due either to the presence of *Hoxa* transcripts in the epithelias (endoderm and ectoderm) (Fig. 6A), to a minimal function of *Hoxd* genes following their sustained expression or to the existence of differences in gene regulatory networks between PA1 and PA2 to PA4, which implies *Dlx*, *Hand2*, and *Msx* genes (Beverdam et al., 2002; Depew et al., 2002; Depew et al., 2005; Vieux-Rochas et al., 2010). However, while the *HoxA* and *HoxB* clusters have redundant roles, they also display specific functions as illustrated by the requirement of *Hoxb* genes either to restrict

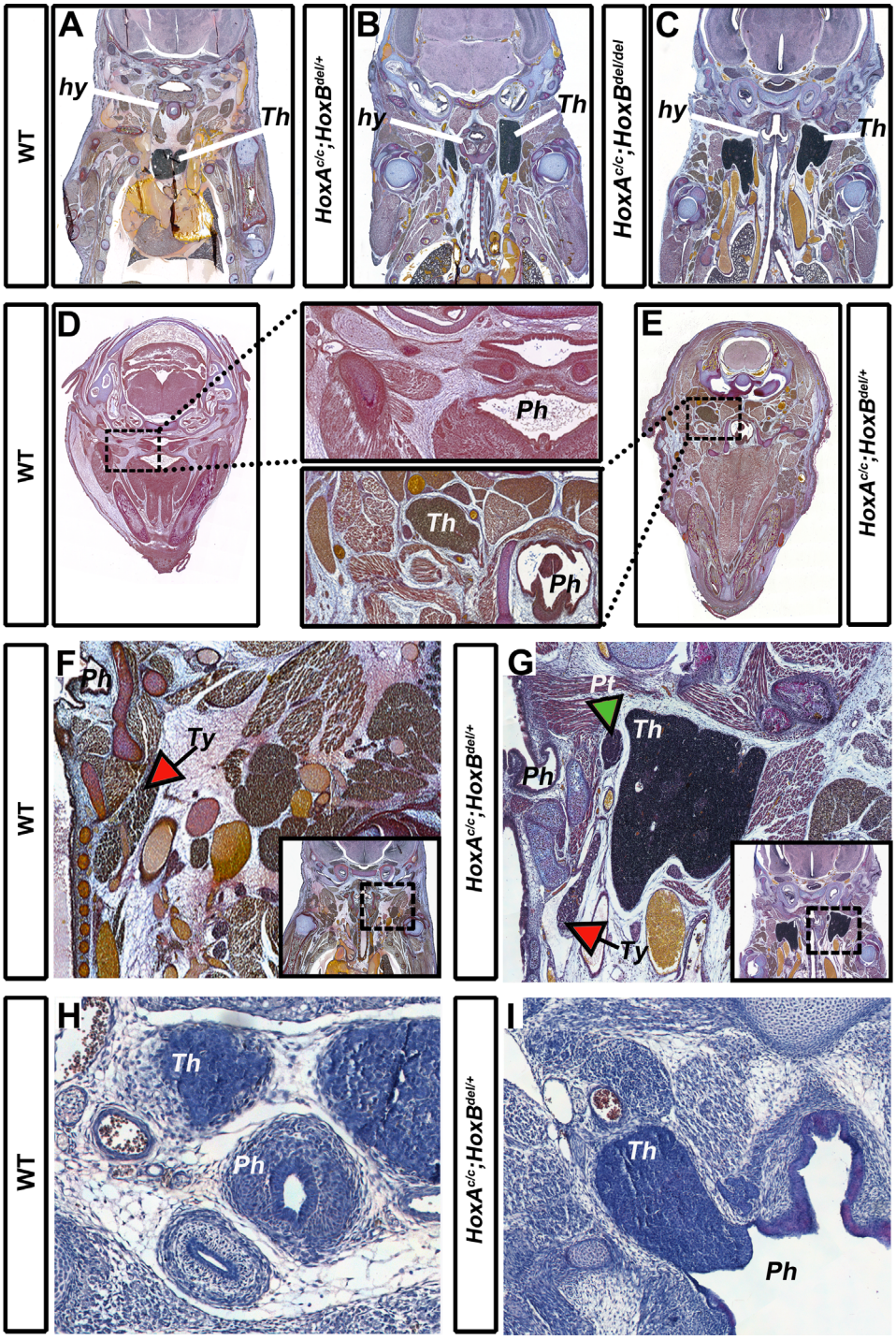

Fig. 5. Ectopic and hypertrophic thymus. (A–C) Hypertrophic thymuses are present in both *HoxA*$^{c/c}$;*HoxB*$^{del/+}$;*wnt-cre* (B) and *HoxA*$^{c/c}$;*HoxB*$^{del/del}$;*wnt-cre* (**C**) mutant embryos. In wild-type specimen (A), the thymus (*Th*) is located in the anterior mediasta. Hypertrophic thymuses in the *HoxA*$^{c/c}$;*HoxB*$^{del/+}$;*wnt-cre* (B) and *HoxA*$^{c/c}$; *HoxB*$^{del/del}$;*wnt-cre* (C) mutants are at the expected place, around the anterior mediasta, but they are also in close contact with the hyoid bone (*Hy*). (D, E) Absence of junction between the thymus and the pharynx in wild-type (D) and in *HoxA*$^{c/c}$;*HoxB*$^{del/+}$;*wnt-cre* (E) mutant embryos at E18,5. (F,G) In E18.5 mutant embryos, the thyroid gland (*Ty,* red arrow) is normally positioned, in close contact with the thyroid bone, whereas the parathyroid gland (*Pt,* green arrowhead) is close to the rostral part of the ectopic thymus. (H, I) Persistent attachment of the thymus to the pharynx in *HoxA*$^{c/c}$;*HoxB*$^{del/+}$;*wnt-cre* mutant embryos. At E15.5, the wild type thymus is located lateral to the pharynx, whereas it is still attached to the pharynx in the mutant embryos (arrow). *hy*: hyoid bone; *Ph*: pharynx; *Pt*: Parathyroid; *Th*: thymus; *Ty*: thyroid.

the formation of component of the middle ear, or in the detachment of the thymus from the pharynx.

In an evolutionary context, the transformation of PA2 structures into the identity of PA1 suggests that the functional abrogation of *Hox* functions in NCCs leads to an extension of PA1 ground-state identity towards more caudal domains (Refs. in Minoux and Rijli (2010)). The acquisition by crest cells of a skeletogenic potential, in parallel with the absence of *Hox* function, may somewhat reflect a fundamental ancestral mechanism, which helped to produce a bona-fide head by selectively repressing *Hox* gene transcription in the most rostral part of the body. In this view, an original contingent of NCCs (or their ancestral forms) may have first appeared in the most rostral part of the body only. Such cells were hypothetically devoid of *Hox* functions leading to the morphogenesis of the new

head combined with the presence of the thymus near the filtrating apparatus. Their further migration towards more caudal parts of the body required important modifications in the morphogenetic potential of these cells, which was accompanied by the activation of *Hox* function at caudal levels (Fig. 6D). This is in agreement with the regulation of *Hox* gene expression in CNCCs being independent of their cis-regulatory control in the CNS (Maconochie et al., 1999; Trainor and Krumlauf, 2000).

In the case of the thymus, its ectopic anatomical position in mutant stocks would thus be somewhat reminiscent of its ancestral form (e.g. near the mouth), as recently reported in the case of lampreys (Bajoghli et al., 2011). The caudal migration of this organ would have been paralleled by an anteriorisation of *Hox* functions into PA2, an information lacking in more ancestral species. This gain of function of *Hox* complements into PA2 could have been instrumental in the functional shift of the thymus from a position near the filtrating organ towards an organ involved in the immune response (Fig. 6D).

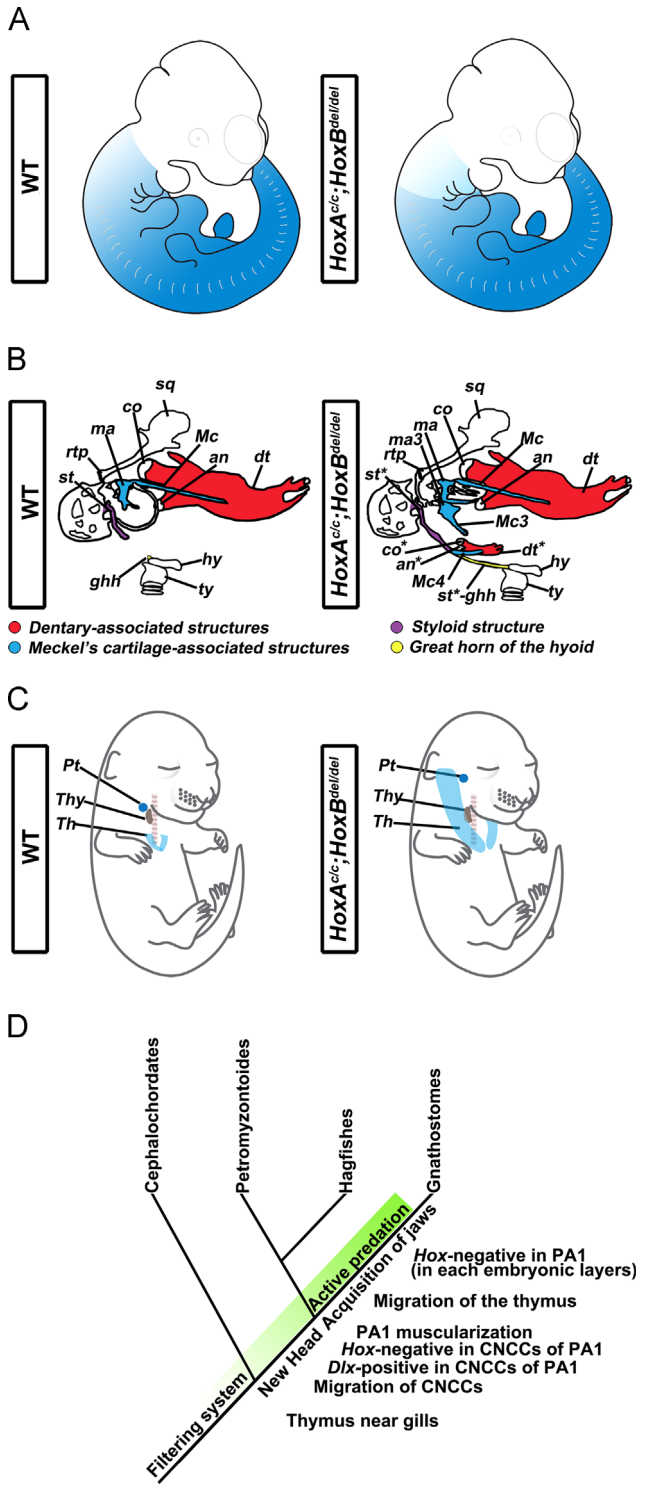

Fig. 6. Potential implications of the HoxA;HoxB double mutant phenotypes to help understand the evolution of neck and jaw. (A) Extent of *Hox* function in E10,5 old embryos. In the wild-type (left), *Hox* genes are expressed from the tail bud up to the second branchial arch (left, blue). In *HoxA*$^{c/c}$;*HoxB*$^{del/del}$;*wnt-cre* mutant embryos, however, *HoxA* and *HoxB* gene functions are depleted from the CNCCs contingent, yet *Hoxa* functions are still present in the epithelial compartments. Also, both, *HoxC* and *HoxD* clusters are still functional (right, light blue). (B) The effects of this functional depletion are summarized with drawings of skeletal and cartilagenous modifications in NCC derivatives. The duplicated dentary bone contacts the styloid and the great horn of the hyoid *via* a supernumerary cartilage, which is interpreted as a quadruplicated Meckel's cartilage. (C) Schemes of the positions of the thymus, parathyroid and thyroid glands. While the thyroid gland shows a normal migration in mutant embryos (right, brown), the parathyroid lies at an ectopic position (right, blue dot). In the *HoxA*$^{c/c}$;*HoxB*$^{del/del}$;*wnt-cre* mutant embryos, the thymus is hypertrophic and has a normal position in the anterior mediasta, yet it extends up to an ectopic position near the hyoid bone (right, light blue). (D) A possible evolutionary scenario for neck and jaw formation based on a recent study on cyclostomes evolution (Oisi et al., 2013). *an*: angular process; *an**: duplicated angular process; *co*: condylar process; *co**: duplicated condylar process; *dt*: dentary; *dt**: duplicated dentary bone; *hy:* hyoid bone; *ma*: malleus; *ma3*: triplicated malleus; *Mc*: Meckel's cartilage; *Mc2*: duplicated Meckel's cartilage; *Mc3**: triplicated Meckel's cartilage; *Mc4**: quadruplicated Meckel's cartilage; *Ph*: pharynx; *Pt*: Parathyroid; *pt*: pterygoid bone; *rtp*: retrotympanic process; *sq*: squamosal bone; *st*: styloid; *st**: stapes-like; *st***-ghh*: stylo-like-great horn hyoid juction; *Th*: thymus; *Ty*: thyroid; *ty*: tympanic bone.

Acknowledgments

We thank Dr. P. Janvier and Dr. M. Mark for helpful discussions on the phenotypes and H. Nguyen Huynh, S. Gitto and J. Codourey for help with mice. We also thank members of the Duboule laboratories for discussions and Dr. M. Renaud for help with drawings. This work was supported by funds from the Ecole Polytechnique Fédérale in Lausanne, the University of Geneva, the Swiss National Research Fund, the National Research Center (NCCR) "Frontiers in Genetics", the EU program "Crescendo" and the ERC grant Systems*Hox*.ch (to D.D.).

Appendix A. Supporting information

Supplementary data associated with this article can be found in the online version at http://dx.doi.org/10.1016/j.ydbio.2013.06.027.

References

Bajoghli, B., Guo, P., Aghaallaei, N., Hirano, M., Strohmeier, C., McCurley, N., Bockman, D.E., Schorpp, M., Cooper, M.D., Boehm, T., 2011. A thymus candidate in lampreys. Nature 470, 90–94.

Beverdam, A., Merlo, G.R., Paleari, L., Mantero, S., Genova, F., Barbieri, O., Janvier, P., Levi, G., 2002. Jaw transformation with gain of symmetry after Dlx5/Dlx6 inactivation: mirror of the past? Genesis 34, 221–227.

Carpenter, E.M., Goddard, J.M., Chisaka, O., Manley, N.R., Capecchi, M.R., 1993. Loss of Hox-A1 (Hox-1.6) function results in the reorganization of the murine hindbrain. Development 118, 1063–1075.

Chen, L., Zhao, P., Wells, L., Amemiya, C.T., Condie, B.G., Manley, N.R., 2010. Mouse and zebrafish Hoxa3 orthologues have nonequivalent in vivo protein function. Proc. Natl. Acad. Sci. USA 107, 10555–10560.

Chisaka, O., Capecchi, M.R., 1991. Regionally restricted developmental defects resulting from targeted disruption of the mouse homeobox gene hox-1.5. Nature 350, 473–479.

Condie, B.G., Capecchi, M.R., 1994. Mice with targeted disruptions in the paralogous genes hoxa-3 and hoxd-3 reveal synergistic interactions. Nature 370, 304–307.
Couly, G., Creuzet, S., Bennaceur, S., Vincent, C., Le Douarin, N.M., 2002. Interactions between Hox-negative cephalic neural crest cells and the foregut endoderm in patterning the facial skeleton in the vertebrate head. Development 129, 1061–1073.
Couly, G., Grapin-Botton, A., Coltey, P., Ruhin, B., Le Douarin, N.M., 1998. Determination of the identity of the derivatives of the cephalic neural crest: incompatibility between Hox gene expression and lower jaw development. Development 125, 3445–3459.
Couly, G.F., Coltey, P.M., Le Douarin, N.M., 1993. The triple origin of skull in higher vertebrates: a study in quail-chick chimeras. Development 117, 409–429.
Creuzet, S., Couly, G., Le Douarin, N.M., 2005. Patterning the neural crest derivatives during development of the vertebrate head: insights from avian studies. J. Anat. 207, 447–459.
Danielian, P.S., Muccino, D., Rowitch, D.H., Michael, S.K., McMahon, A.P., 1998. Modification of gene activity in mouse embryos in utero by a tamoxifen-inducible form of Cre recombinase. Curr. Biol. 8, 1323–1326.
Depew, M.J., Lufkin, T., Rubenstein, J.L., 2002. Specification of jaw subdivisions by Dlx genes. Science 298, 381–385.
Depew, M.J., Simpson, C.A., Morasso, M., Rubenstein, J.L., 2005. Reassessing the Dlx code: the genetic regulation of branchial arch skeletal pattern and development. J. Anat. 207, 501–561.
Dooley, J., Erickson, M., Gillard, G.O., Farr, A.G., 2006. Cervical thymus in the mouse. J. Immunol. 176, 6484–6490.
Eagle, W.W., 1949. Symptomatic elongated styloid process; report of two cases of styloid process-carotid artery syndrome with operation. Arch. Otolaryngol. 49, 490–503.
Foster, K.E., Gordon, J., Cardenas, K., Veiga-Fernandes, H., Makinen, T., Grigorieva, E., Wilkinson, D.G., Blackburn, C.C., Richie, E., Manley, N.R., Adams, R.H., Kioussis, D., Coles, M.C., 2010. EphB-ephrin-B2 interactions are required for thymus migration during organogenesis. Proc. Natl. Acad. Sci. USA 107, 13414–13419.
Gammill, L.S., Bronner-Fraser, M., 2002. Genomic analysis of neural crest induction. Development 129, 5731–5741.
Gavalas, A., Trainor, P., Ariza-McNaughton, L., Krumlauf, R., 2001. Synergy between Hoxa1 and Hoxb1: the relationship between arch patterning and the generation of cranial neural crest. Development 128, 3017–3027.
Gendron-Maguire, M., Mallo, M., Zhang, M., Gridley, T., 1993. Hoxa-2 mutant mice exhibit homeotic transformation of skeletal elements derived from cranial neural crest. Cell 75, 1317–1331.
Grevellec, A., Tucker, A.S., 2010. The pharyngeal pouches and clefts: Development, evolution, structure and derivatives. Semin. Cell Dev. Biol. 21, 325–332.
Hunter, M.P., Prince, V.E., 2002. Zebrafish hox paralogue group 2 genes function redundantly as selector genes to pattern the second pharyngeal arch. Dev. Biol. 247, 367–389.
Kmita, M., Tarchini, B., Zakany, J., Logan, M., Tabin, C.J., Duboule, D., 2005. Early developmental arrest of mammalian limbs lacking HoxA/HoxD gene function. Nature 435, 1113–1116.
Kontges, G., Lumsden, A., 1996. Rhombencephalic neural crest segmentation is preserved throughout craniofacial ontogeny. Development 122, 3229–3242.
Kuraku, S., Meyer, A., Kuratani, S., 2009. Timing of genome duplications relative to the origin of the vertebrates: did cyclostomes diverge before or after? Mol. Biol. Evol. 26, 47–59.
Kuratani, S., 2012. Evolution of the vertebrate jaw from developmental perspectives. Evol. Dev. 14, 76–92.
Kuratani, S., Adachi, N., Wada, N., Oisi, Y., Sugahara, F., 2013. Developmental and evolutionary significance of the mandibular arch and prechordal/premandibular cranium in vertebrates: revising the heterotopy scenario of gnathostome jaw evolution. J. Anat. 222, 41–55.
Lam, S.H., Chua, H.L., Gong, Z., Wen, Z., Lam, T.J., Sin, Y.M., 2002. Morphologic transformation of the thymus in developing zebrafish. Dev. Dyn. 225, 87–94.
Le Douarin, N.M., Dieterlen-Lievre, F., Oliver, P.D., 1984. Ontogeny of primary lymphoid organs and lymphoid stem cells. Am. J. Anat. 170, 261–299.
Maconochie, M., Krishnamurthy, R., Nonchev, S., Meier, P., Manzanares, M., Mitchell, P.J., Krumlauf, R., 1999. Regulation of Hoxa2 in cranial neural crest cells involves members of the AP-2 family. Development 126, 1483–1494.
Manley, N.R., Capecchi, M.R., 1997. Hox group 3 paralogous genes act synergistically in the formation of somitic and neural crest-derived structures. Dev. Biol. 192, 274–288.
Manley, N.R., Capecchi, M.R., 1998. Hox group 3 paralogs regulate the development and migration of the thymus, thyroid, and parathyroid glands. Dev. Biol. 195, 1–15.
Mark, M., Lufkin, T., Vonesch, J.L., Ruberte, E., Olivo, J.C., Dolle, P., Gorry, P., Lumsden, A., Chambon, P., 1993. Two rhombomeres are altered in Hoxa-1 mutant mice. Development 119, 319–338.
Medina-Martinez, O., Bradley, A., Ramirez-Solis, R., 2000. A large targeted deletion of Hoxb1-Hoxb9 produces a series of single-segment anterior homeotic transformations. Dev. Biol. 222, 71–83.
Meulemans, D., Bronner-Fraser, M., 2004. Gene-regulatory interactions in neural crest evolution and development. Dev. Cell 7, 291–299.
Miguez, A., Ducret, S., Di Meglio, T., Parras, C., Hmidan, H., Haton, C., Sekizar, S., Mannioui, A., Vidal, M., Kerever, A., Nyabi, O., Haigh, J., Zalc, B., Rijli, F.M., Thomas, J.L., 2012. Opposing roles for Hoxa2 and Hoxb2 in hindbrain oligodendrocyte patterning. J. Neurosci.: Off. J. Soc. Neurosci. 32, 17172–17185.
Milet, C., Monsoro-Burq, A.H., 2012. Neural crest induction at the neural plate border in vertebrates. Dev. Biol. 366, 22–33.
Minoux, M., Antonarakis, G.S., Kmita, M., Duboule, D., Rijli, F.M., 2009. Rostral and caudal pharyngeal arches share a common neural crest ground pattern. Development 136, 637–645.
Minoux, M., Rijli, F.M., 2010. Molecular mechanisms of cranial neural crest cell migration and patterning in craniofacial development. Development 137, 2605–2621.
O'Gorman, S., 2005. Second branchial arch lineages of the middle ear of wild-type and Hoxa2 mutant mice. Dev. Dyn. 234, 124–131.
Oisi, Y., Ota, K.G., Kuraku, S., Fujimoto, S., Kuratani, S., 2013. Craniofacial development of hagfishes and the evolution of vertebrates. Nature 493, 175–180.
Owen, R., 1886. On the Anatomy of Vertebrates. Volume 1: Fishes and Reptiles,. Longmans, Green and Co, London.
Prasad, M.S., Sauka-Spengler, T., LaBonne, C., 2012. Induction of the neural crest state: control of stem cell attributes by gene regulatory, post-transcriptional and epigenetic interactions. Dev. Biol 366, 10–21.
Ravi, V., Lam, K., Tay, B.H., Tay, A., Brenner, S., Venkatesh, B., 2009. Elephant shark (*Callorhinchus milii*) provides insights into the evolution of Hox gene clusters in gnathostomes. Proc. Natl. Acad. Sci. USA 106, 16327–16332.
Rijli, F.M., Mark, M., Lakkaraju, S., Dierich, A., Dolle, P., Chambon, P., 1993. A homeotic transformation is generated in the rostral branchial region of the head by disruption of Hoxa-2, which acts as a selector gene. Cell 75, 1333–1349.
Rinon, A., Lazar, S., Marshall, H., Buchmann-Moller, S., Neufeld, A., Elhanany-Tamir, H., Taketo, M.M., Sommer, L., Krumlauf, R., Tzahor, E., 2007. Cranial neural crest cells regulate head muscle patterning and differentiation during vertebrate embryogenesis. Development 134, 3065–3075.
Rossel, M., Capecchi, M.R., 1999. Mice mutant for both Hoxa1 and Hoxb1 show extensive remodeling of the hindbrain and defects in craniofacial development. Development 126, 5027–5040.
Santagati, F., Rijli, F.M., 2003. Cranial neural crest and the building of the vertebrate head. Nat. Rev. Neurosci. 4, 806–818.
Sauka-Spengler, T., Bronner-Fraser, M., 2008. Evolution of the neural crest viewed from a gene regulatory perspective. Genesis 46, 673–682.
Sauka-Spengler, T., Meulemans, D., Jones, M., Bronner-Fraser, M., 2007. Ancient evolutionary origin of the neural crest gene regulatory network. Dev. Cell 13, 405–420.
Shimeld, S.M., Donoghue, P.C., 2012. Evolutionary crossroads in developmental biology: cyclostomes (lamprey and hagfish). Development 139, 2091–2099.
Smith, J.J., Kuraku, S., Holt, C., Sauka-Spengler, T., Jiang, N., Campbell, M.S., Yandell, M.D., Manousaki, T., Meyer, A., Bloom, O.E., Morgan, J.R., Buxbaum, J.D., Sachidanandam, R., Sims, C., Garruss, A.S., Cook, M., Krumlauf, R., Wiedemann, L.M., Sower, S.A., Decatur, W.A., Hall, J.A., Amemiya, C.T., Saha, N.R., Buckley, K. M., Rast, J.P., Das, S., Hirano, M., McCurley, N., Guo, P., Rohner, N., Tabin, C.J., Piccinelli, P., Elgar, G., Ruffier, M., Aken, B.L., Searle, S.M., Muffato, M., Pignatelli, M., Herrero, J., Jones, M., Brown, C.T., Chung-Davidson, Y.-W., Nanlohy, K.G., Libants, S.V., Yeh, C.-Y., McCauley, D.W., Langeland, J.A., Pancer, Z., Fritzsch, B., de Jong, P.J., Zhu, B., Fulton, L.L., Theising, B., Flicek, P., Bronner, M.E., Warren, W. C., Clifton, S.W., Wilson, R.K., Li, W., 2013. Sequencing of the sea lamprey (*Petromyzon marinus*) genome provides insights into vertebrate evolution. Nat. Genet. 45, 415–421, 421e411–412.
Soshnikova, N., Dewaele, R., Janvier, P., Krumlauf, R., Duboule, D., 2013. Duplications of hox gene clusters and the emergence of vertebrates. Dev Biol 378, 194–199.
Theveneau, E., Mayor, R., 2012. Neural crest delamination and migration: from epithelium-to-mesenchyme transition to collective cell migration. Dev. Biol. 366, 34–54.
Trainor, P.A., Krumlauf, R., 2000. Patterning the cranial neural crest: hindbrain segmentation and Hox gene plasticity. Nat. Rev. Neurosci. 1, 116–124.
Vieux-Rochas, M., Coen, L., Sato, T., Kurihara, Y., Gitton, Y., Barbieri, O., Le Blay, K., Merlo, G., Ekker, M., Kurihara, H., Janvier, P., Levi, G., 2007. Molecular dynamics of retinoic acid-induced craniofacial malformations: implications for the origin of gnathostome jaws. PLoS One 2, e510.
Vieux-Rochas, M., Mantero, S., Heude, E., Barbieri, O., Astigiano, S., Couly, G., Kurihara, H., Levi, G., Merlo, G.R., 2010. Spatio-temporal dynamics of gene expression of the Edn1-Dlx5/6 pathway during development of the lower jaw. Genesis 48, 262–373.
Yu, J.K., Meulemans, D., McKeown, S.J., Bronner-Fraser, M., 2008. Insights from the amphioxus genome on the origin of vertebrate neural crest. Genome Res. 18, 1127–1132.